Solar Energy 159 (2018) 66–77

Contents lists available at ScienceDirect

Solar Energy

journal homepage: www.elsevier.com/locate/solener

Solar furnace temperature control with active cooling☆

Bertinho A. Costa[a,*], João M. Lemos[a], Emmanuel Guillot[b]

[a] INESC-ID/IST, University of Lisbon, Rua Alves Redol, 9, 1000-029, Portugal
[b] CNRS-PROMES, 7 rue du Four Solaire, 66120 Font Romeu Odeillo, France

ARTICLE INFO

Keywords:
Solar thermal energy
Solar furnace
Modelling
Control
Active cooling

ABSTRACT

The article describes a control architecture for solar furnaces where active cooling is employed to improve the tracking of a time-varying temperature reference. This capability is important during the decreasing phase of the temperature reference where heat loss must be increased. The results of two different control methodologies, exact linearization and model predictive control with integral action, are shown with active cooling that is done in coordination with the command of the shutter which adjusts the solar incident power.

The controller parameters are computed from the temperature dynamics which is identified off-line from collected process data. This approach is used to avoid online adaptation mechanisms of the controller parameters, that may cause stability problems during the controller startup, and may melt the testing material sample.

The novelty of the present work is to present a control architecture that coordinates the operations of the shutter together with the application of active cooling. This methodology improves temperature reference tracking and increases the usability and the operation of solar furnaces.

1. Introduction

Increased energy costs, past energy crises and energy conflicts, carbon-based energy pollution, and the expected fossil-fuels induced climate changes, have triggered the development of renewable energy technologies such as concentrating solar power systems (CSP). CSP include solar furnaces, photovoltaic (CPV), solar thermal (CST) which have a wide application, such as the “generation” of electrical energy and heat (Camacho et al., 2007a,b), the production of solar fuels, hydrogen and syngas (Agrafiotis et al., 2014), desalinization, and material processing (Oliveira et al., 2015, 2016).

The article addresses the control of solar furnaces for material processing and stress testing, where the temperature of the sample must follow a time-varying reference with precision. The proposed control architecture has a cascade structure where the outer controller is employed to control the temperature of the sample, computes a reference for the incident flux on the sample, and supplies it to the inner controller. The inner controller adjusts the position of the shutter using the information that it receives from the temperature controller and compensates changes present in the solar irradiance. If needed, solar incident flux control experiments can be done using only the inner controller.

Research on control of solar furnaces for material processing and stress testing, developed at the Plataforma Solar de Almeria (Berenguel et al., 1999), have addressed several topics, such as constrained temperature control and disturbance rejection (Beschi et al., 2012, 2013b), linearization with the Generalized Predictive Control (GPC) algorithm (Beschi et al., 2013a) and fractional robust PID control (Beschi et al., 2016).

Motivated by the improvement of operation and automation of small size solar furnaces at PROMES, Odeillo, (France) to obtain repeatable results that do not depend on the human operator that manually controls the experiment, several control strategies have been developed and tested, such as adaptive control (Costa and Lemos, 2009a,b; Costa et al., 2011), predictive adaptive temperature control (Costa and Lemos, 2012), and optimal control (Costa and Lemos, 2016). The work that is presented in this article is based on the previous works (Costa et al., 2016a,b) but has the novelty of considering active cooling to improve temperature reference tracking, in particular when the shutter is closed and the temperature of the sample is above the reference temperature. It is interesting to remark that, by including active cooling to operate when active heating is off and the temperature of the sample is above the temperature reference, a switched temperature dynamics is obtained. The details are described in Section 2.

The article is organized as follows: in Section 2 a description of the

☆ This work was partially supported by the European Union through project SFERA2, under FP7 (project number 312643) and by the FCT-Portugal under the contract UID/CEC/50021/2013.

* Corresponding author.
E-mail addresses: bac@inesc-id.pt (B.A. Costa), jlml@inesc-id.pt (J.M. Lemos), emmanuel.guillot@promes.cnrs.fr (E. Guillot).

http://dx.doi.org/10.1016/j.solener.2017.10.017
Received 16 June 2017; Received in revised form 28 September 2017; Accepted 4 October 2017

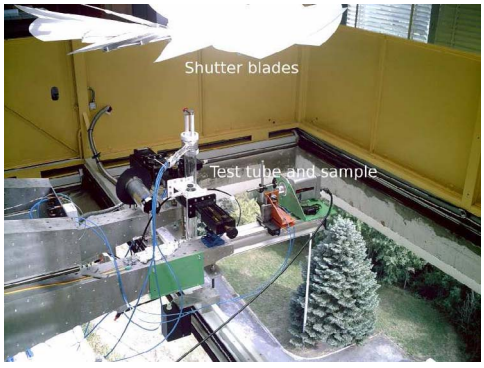

(a) Shutter of the 6kW solar furnace.

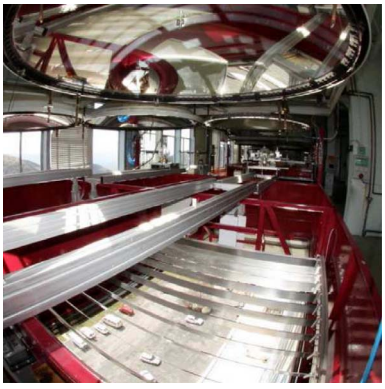

(b) The 1.5kW solar furnace with a sesame shutter

Fig. 1. Examples of solar furnaces at PROMES with different shutters, located after and before the concentrating flux.

solar furnace and its model are presented; in Section 3 the identification of the process is described and some results are shown; in Section 4 the control system architecture is described and the stability of the switching control is addressed; Sections 5 and 6 show experimental results obtained with several materials and with two control methodologies, *viz.* exact linearization and model predictive control, that includes the application of active cooling to improve the temperature reference tracking; the conclusions are presented in Section 7. Details of the two control methodologies are described in appendix.

2. Solar furnace model

The solar furnace model used in this work comprises three models, namely a temperature model that describes the thermodynamic relation between the temperature of the sample and the amount of heat applied (removed) to (from) the material sample, a model that describes the action of the shutter to heat the sample, and a model that describes the function of the blower/fan employed to remove heat from the sample.

2.1. Shutter model

A shutter, see Fig. 1, is employed to adjust the amount of solar power that is applied to the upper surface of a sample. This objective is achieved by adjusting the position the shutter blades, see Fig. 2, that constrain the amount of irradiance at the focus of the solar furnace. The shutter operates in closed loop and its dynamics is much faster than the thermal dynamics. The controller of the shutter is able to move the blades to the target angle in less than 0.2 s. Thus, in this work, only the static function of the shutter is considered, being

$$s_{fs}(u_s(t)) = 1 - \frac{\cos(\theta_0 + u_s(t)(90° - \theta_0)/100)}{\cos(\theta_0)}, \tag{1}$$

where the shutter command is physically constrained to $0 \leqslant u_s(t) \leqslant 100$ and $\theta_0 = 25°$. This assumption must be considered in the design of the controllers since otherwise the control performance may be unacceptable (Costa and Lemos, 2009b).

2.2. Blower/fan model

The bowler/fan is employed to remove heat from the sample. The amount of heat that is removed by forced convection is described by

$$\dot{Q}r_f = h_a A_s [T_s(t) - T_e(t)], \tag{2}$$

where $T_s(\cdot)$ [K] represents the temperature of the sample, T_e [K] represents the temperature of the air that flows on the sample, h_a represents the average convection heat transfer coefficient (that depends on the massic air flow), and A_s is the heat transfer surface area.

The forced convection heat transfer coefficient, h_a, is described by the correlations (Çengel, 2003) involving the Nusselt number ($N_{uL} = h_a L/k$), the Reynolds number ($R_{eL} = VL/\nu$) and the Prandlt number (P_r can be considered constant (0.73) for the temperature interval [20 °C; 2000 °C] of the experiments),

$$h_a = \frac{k}{L}\left(\frac{VL}{\nu}\right)^m P_r^n, \tag{3}$$

where L is the "length" of the material sample, k represents the thermal conductivity of the fluid (air), ν is the kinematic viscosity of the fluid, and V is fluid velocity (air). The constants C,m, and n depend on the type of flow, which can be predicted from the Reynolds number. For $R_{eL} < 5 \times 10^5$ the type of flow is laminar and $C = 0.664$, $m = 1/2$, and $n = 1/3$ but in the case of turbulent flow $5 \times 10^5 < R_{eL} < 10^6$ and $C = 0.036$, $m = 4/5$, and $n = 1/3$. The fluid velocity, V, is a function of the blower characteristic and depends on the electric power, (voltage) applied to the blower. Since the blower used has a large hysteresis and a large dead-zone, it was decided to operate/command the blower using an ON($u_{bf} = 100\%$)-OFF ($u_{bf} = 0\%$) strategy, that imposes V in a very short time (1 s). Thus, in the OFF mode $V = 0$, and for the ON mode $V = V_{max}$.

2.3. Temperature model of the sample

Small size samples are usually used to perform stress tests. Typically, a sample has a circular shape with a diameter of 2 cm and a height of 2 mm, but other sizes and shapes were tested. The temperature model is developed based on an energy balance such as the one made in Berenguel et al. (1999), but in this work active heating (shutter operation), and active cooling (blower/fan operation), are considered to improve temperature reference tracking.

In the case of active heating, the temperature of the sample, $T_s(t)$ [K] is approximately described by

$$\frac{dT_s(t)}{dt} = -\alpha_1[T_s^4(t) - T_b^4(t)] - \alpha_2[T_s(t) - T_e(t)] + \alpha_3 G_s(t) s_{fs}(u_s(t)). \tag{4}$$

Here, T_b [K] represents the temperature of the "environment" that contributes to losses by radiation (Berenguel et al., 1999; Çengel, 2003) and T_e represents the temperature of the surrounding air that contributes to losses by natural convection or air flow disturbances. The factors α_1, α_2 and α_3 represent the process parameters, being defined by

$$\alpha_1 = \frac{\epsilon(T_s)\sigma A_{sr}}{C_p(T_s)m}; \ \alpha_2 = \frac{h_{conv}(T_s, T_e)A_{sc}}{C_p(T_s)m}; \ \alpha_3 = \frac{\alpha_s A_{si} g_f}{C_p(T_s)m}, \tag{5}$$

where $h_{conv} = 1.32(T_s - T_e)/L_c$[1] for natural laminar flow. The parameters

[1] With $L_c = 4(Area)/(Perimeter)$ of the sample.

(a) Visualization of the focus of a solar furnace with a water spray.

(b) Setup for control experiments.

Fig. 2. The solar furnaces used to evaluate the coordination of active heating with active cooling.

Table 1
Thermal model parameters.

Parameter: Description
ρ [kg m^{-3}]: Density of the material
C_p [J kg^{-1} K^{-1}]: Material Specific Heat
m [kg]: Mass of the sample
ϵ: Emissivity of the material
σ [W m^{-2} K^{-4}]: Stefan–Boltzmann const.
A_{sr} [m^2]: Sample's loss radiation area
A_{sc} [m^2]: Sample's convection area
A_{si} [m^2]: Sample's incident area
L_c [m]: Characteristic length
h_{conv} [W m^{-2}K^{-1}]: Convection factor
α_s: Sample's solar absorption factor
g_f: Furnace gain
G_s [W/m^2]: Solar Irradiance

in (5) are described in Table 1. The parameters α_1, α_2, and α_3 are estimated using data collected from the process as shown in Fig. 3, where the shutter was commanded manually to change the temperature of a stainless steel sample. In order to perform the process identification, $G_s(\cdot)$ (available sun power) is also recorded. The sampling period is $h = 0.5$ s.

Using data available in the literature (Çengel, 2003) for known materials, it is concluded that the parameters α_1, α_2, and α_3 depend, in a "small" degree, on the temperature and the dependence can be mitigated by using an adequate control structure. The model identification is used to obtain the "mean values" of the parameters (active heating model) for the temperature range considered. It is important to mention that the properties of a new material are not known and the characteristic of the blower/fan is not known. But if the dependence on the temperature is large, it is possible to use linear or quadratic equations to approximate the temperature dependence. This fact implies the identification of a large set of parameters and one must be aware of a possible parameter identifiability problem. Thus the approach proposed is to keep the process model (active heating) simple and to validate the off-line identification by comparing the output of the model with the collected data. From the control point of view it is important to use a simple model that captures the main dynamics and to use a control strategy that is able to cope not only with constant process parameters but is able to yield a good control performance in the presence of small parameter changes when compared with the range of the variable to be controlled. This goal can only be achieved by testing the proposed control architecture in real conditions.

In the case of active cooling, the shutter is closed and the blower/fan is operated to remove heat from the sample. This action will be used only if the shutter is closed, and the temperature of the sample is above the temperature reference. In this case the temperature of the sample is described by

$$\frac{dT_s(t)}{dt} = -\alpha_1[T_s^4(t) - T_b^4(t)] - \alpha_f(u_{bf}(t))[T_s(t) - T_e(t)], \tag{6}$$

where $u_{bf}(\cdot)$ represents the command of the blower/fan.

From the description made about the process it is concluded that there are two operating modes, namely the active heating mode (that corresponds to losses by natural convection and heat applied using the shutter) and the active cooling mode (where the blower is used to remove heat). This approach can be envisage from different perspectives. From the actuation point of view, a "composed" actuator can be considered that joins two different characteristics, the heating characteristic (natural convection plus the shutter operation) and the characteristic to remove heat (forced convection). But if one considers the process dynamics, the two operating modes have different differential equations, (4) and (6), where the magnitude of $\alpha_2[T_s(t) - T_e(t)]$ and $\alpha_f(u_{bf}(t))[T_s(t) - T_e(t)]$ are very different and this depends on the operating mode, active heating or with active cooling. This model can be seen as a process with switched dynamics (see Fig. 4).

3. Off-line identification of the temperature model

3.1. Identification of the temperature model with the shutter input

In order to estimate the parameters α_1, α_2, and α_3, these are assumed to be constant, and sampled data is used. The continuous time model is transformed, a first order filter is employed, and a conversion to a discrete time model is performed. The following signals are defined, $\zeta_1(t) = [T_s^4(t) - T_e^4(t)]$, $\zeta_2(t) = [T_s(t) - T_e(t)]$, and $\zeta_3(t) = u_r(t) = G_s(t)s_{fs}(u_s(t))$, and a stable low-pass filter $O(s) = a/(s + a)$ with unitary static gain is applied to (4), yielding

$$\frac{as}{(s+a)}T_s(s) = -\alpha_1\frac{a\zeta_1(s)}{(s+a)} - \alpha_2\frac{a\zeta_2(s)}{(s+a)} + \alpha_3\frac{a\zeta_3(s)}{(s+a)}. \tag{7}$$

The value of parameter $a > 0$ is selected based on the level of noise present on $T_s(\cdot)$ and on the dynamics of the process. The general rule is to select the filter to be much faster than the temperature dynamics. It follows that (7) admits the continuous time representation

$$\zeta_{f0}(t) = -\alpha_1\zeta_{f1}(t) - \alpha_2\zeta_{f2}(t) + \alpha_3\zeta_{f3}(t), \tag{8}$$

with

$$\frac{dT_{sf}(t)}{dt} = -aT_{sf}(t) + aT_s(t), \tag{9}$$

$$\zeta_{f0}(t) = a(T_s(t) - T_{sf}(t)), \tag{10}$$

$$\frac{d\zeta_{f1}(t)}{dt} = -a\zeta_{f1}(t) + a\zeta_1(t), \tag{11}$$

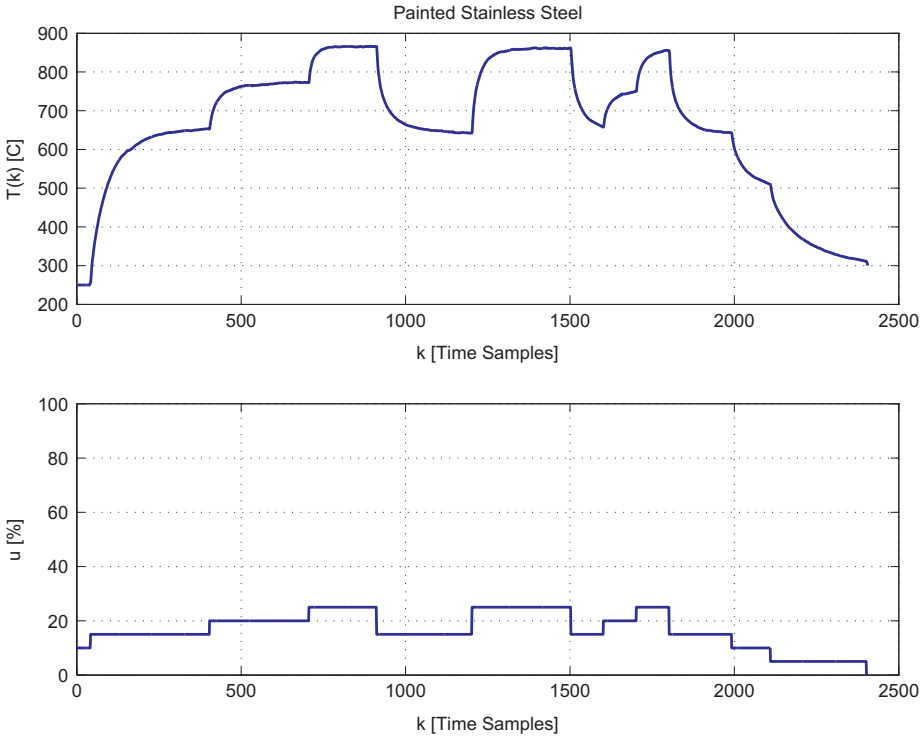

Fig. 3. Data collected from the solar furnace by manually adjusting the shutter. The material sample temperature is shown at the top and the manipulated variable is shown at the bottom. The solar power was almost constant during the experiment (950 W/m^2).

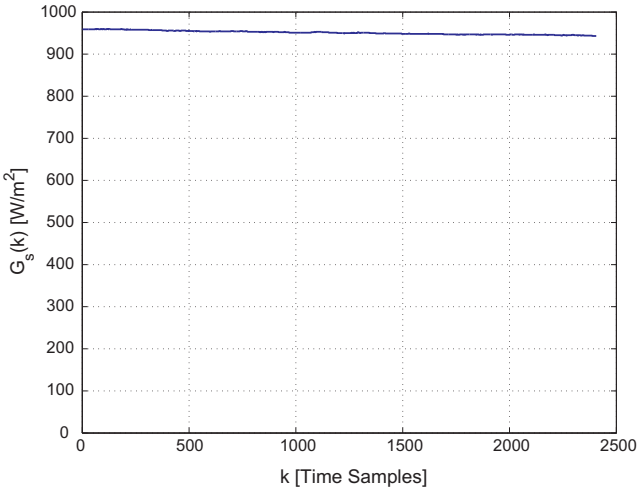

Fig. 4. Solar power during the experiment to collect data for model identification, corresponding to Fig. 3.

$$\frac{d\zeta_{f2}(t)}{dt} = -a\zeta_{f2}(t) + a\zeta_2(t), \tag{12}$$

$$\frac{d\zeta_{f3}(t)}{dt} = -a\zeta_{f3}(t) + a\zeta_3(t). \tag{13}$$

In order to solve these dynamic equations in discrete time, the first order hold (FOH) method is applied using the sampling time $h = 0.5$ s, the continuous time variable[2] t is related to the discrete time variable k by $t = t_0 + kh$, where t_0 that represents time when the experiment starts, but can be equal to zero. The estimation of parameters α_1, α_2, and α_3 are computed with the Least Mean Square (LMS) method using the discrete time signals $\zeta_{f0}[k]$, $\zeta_{f1}[k]$, $\zeta_{f2}[k]$, and $\zeta_{f3}[k]$.

Considering Eq. (8) and the data at each sample time, and considering a time window of size $n + 1$, it follows that

$$\begin{bmatrix} y[k] \\ y[k-1] \\ \cdots \\ y[k-n] \end{bmatrix} = \begin{bmatrix} \zeta_{f1}[k] & \zeta_{f2}[k] & \zeta_{f3}[k] \\ \zeta_{f1}[k-1] & \zeta_{f2}[k-1] & \zeta_{f3}[k-1] \\ \cdots & \cdots & \cdots \\ \zeta_{f1}[k-n] & \zeta_{f2}[k-n] & \zeta_{f3}[k-n] \end{bmatrix} \begin{bmatrix} \alpha_1 \\ \alpha_2 \\ \alpha_3 \end{bmatrix}, \tag{14}$$

that can be represented as $Y = \Phi\alpha$. The parameters estimates are obtained from

$$\alpha = (\Phi^T\Phi)^{-1}\Phi Y, \tag{15}$$

where the matrix $\Phi^T\Phi$ must have inverse. The validity of this assumption depends on the spectrum content of the control signal that must be "rich" enough. In the present work, the shutter is operated by steps to evaluate the time response of the (material sample) temperature. Note that, in the present problem, there is a huge difference between the numerical values of $\zeta_{f1}[k]$ $\zeta_{f2}[k]$ $\zeta_{f3}[k]$, that depend on $T^4(\cdot)$,$T(\cdot)$ and $G_s(\cdot)s_{fs}(u_s(\cdot))$, a fact that may cause numerical problems. To solve this problem, the matrix Φ is scaled by a diagonal matrix such that $Y = \Phi\Lambda\alpha_L$, with $\alpha_L = \Lambda^{-1}\alpha$.

The results of the off-line identification corresponding to a time window of Fig. 3 are shown in Fig. 5, where the model output gives a good approximation of the process output $T_s[k]$ (blue[3] colour). It is remarked that the same data has been used for identification and for validation purposes. However, in this particular case this procedure was considered acceptable.

The scaling matrix was selected as $diag(\Lambda) = [2.0 \times 10^{-11}, 1.0 \times 10^{-2}, 1.0 \times 10^{-1}]$, and the estimates of $\overline{\alpha}_1$, $\overline{\alpha}_2$ and $\overline{\alpha}_3$ are respectively, 1.590×10^{-11},1.581×10^{-2},2.608×10^{-1}.

An important aspect that the model can provide is the quantification of the relation between the energy loss by radiation, described by the term $\overline{\alpha}_1[T_s^4[k] - T_e^4[k]]$ that is nonlinear, and the term corresponding to energy loss by convection $\overline{\alpha}_2[T_s[k] - T_e[k]]$, that has a linear contribution to the temperature dynamics. The comparison is presented in Fig. 6,

[2] Notation: In the article $y(t)$ represents a continuous time signal, $y(k)$ or $y[k]$ represents a discrete time signal that is obtained from $y(t)$ by sampling it with a constant sampling time h.

[3] For interpretation of color in Figs. 3 and 9, the reader is referred to the web version of this article.

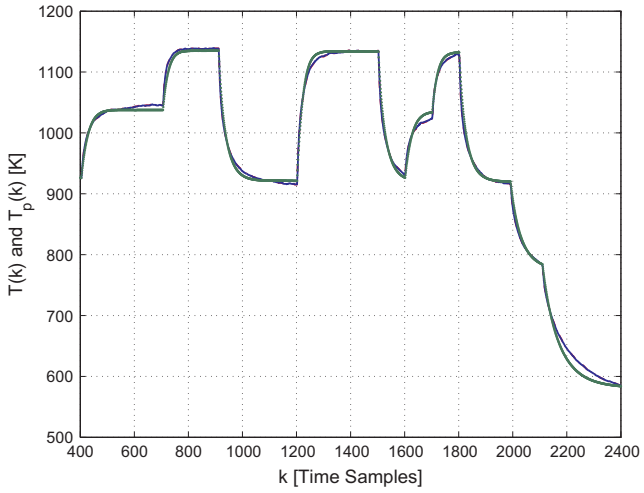

Fig. 5. Off-line model identification. Three signals are shown, the sample temperature $T_s[k]$ collected from the process (blue colour) and the one step-head prediction (red colour), these signals are very similar. The other signal, represented in green colour, is obtained from the temperature model that is initialized with the temperature value $T_s[400]$ and uses the collected data $u_s[k]$ and $G_s[k]$. The model output yields an approximation of the process output that is acceptable for control design purposes. (For interpretation of the references to colour in this figure legend, the reader is referred to the web version of this article.)

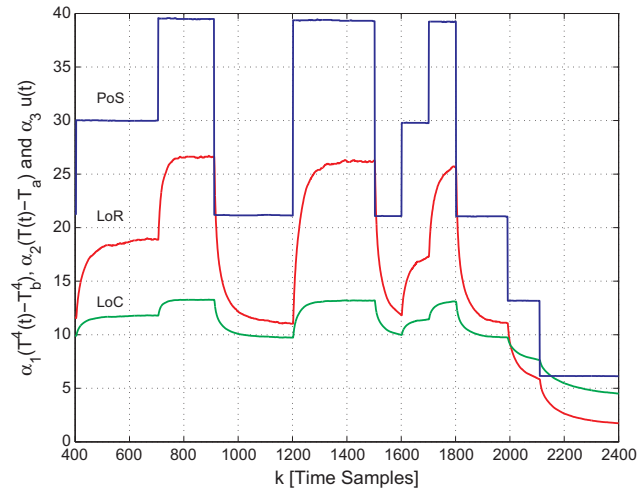

Fig. 6. Comparing the contribution of each term of the temperature model, PoS – Power absorption ($\varpi_3 G_s[k] s_{fs}(u_s[k])$, LoR – Loss by Radiation ($\varpi_1[T_s^4[t]-T_b^4]$) and LoC – Loss by natural Convection ($\varpi_2[T_s(t)-T_e]$). The temperature of the sample for the same time window is shown in Fig. 5.

from which it can be concluded that the nonlinear term dominates for temperatures higher than 900 K. Below this temperature value the energy loss by convection has a bigger contribution to the temperature dynamics.

3.2. Identification of the temperature model with the blower/fan input

The procedure that was describe for the identification of the temperature model with the shutter input can be applied to the model that has the blower/fan input. But due to practical-operational constrains of the fan used, that has a large non-linearity and hysteresis, it was decided to command the fan using an on-off (0–100%) strategy.

The heat loss caused by operating the fan, $\dot{Q}r_f$, was not identified. This uncertainty is addressed in the control design of the solar furnace.

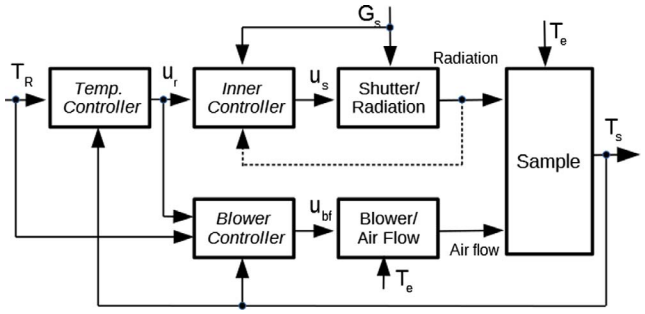

Fig. 7. Control system architecture for the solar furnace with the command of the shutter (heating) and the command of the blower (active cooling). The shutter and the blower do not operate during the same time period.

4. Control system architecture

The control system architecture for the solar furnace is represented in Fig. 7. The temperature controller generates a reference power value $u_r[k]$ that is supplied, according to a cascade structure, to the shutter controller and to the blower controller. These controllers are in two parallel control lines. Since the objective is to perform stress test cycles induced by high temperature levels, the temperature controller and the shutter control line are operating much of the time. The control design is such that the temperature controller stabilizes the closed-loop in the presence of the process input saturations. The blower/fan control line is only used if the reference power value $u_r[k]$ is saturated at 0% and the temperature of the sample is above the reference temperature. This condition means that the temperature controller is trying to remove heat from the sample. The shutter control line and the blower control line are not simultaneously active, that is, they are not active during the same discrete time instant. The proposed architecture is a special case of the so called split-range control (Stephanopoulos, 1984, pp. 404–409).

In order to implement the control system architecture, the temperature controller is first designed with the objective that a null static tracking error is obtained without overshoot. This implies that the controller must have integral action and a mechanism of anti-windup to handle the saturation of $u_r[k]$.

Although several methodologies are available to design the temperature controller, in this work two approaches are used, the concept of exact linearization that is described in Appendix A.1, and the methodology of model predictive control with integral action that is described in Appendix A.2. In the above architecture, it is implicitly assumed that the solar irradiance is constant along the time horizon. The controller described as “shutter controller” is responsible for the solar irradiance compensation.

The switching decision between the two operating modes can be implemented with different rules. In Costa et al. (2016b) the blower/fan is employed when the shutter is closed and temperature of the sample is above the temperature reference ($e_s[k] < 0$). The blower is stopped for $e_s[k] \geqslant 0$. This action can be considered as a disturbance that the temperature controller must compensate.

In this work, instead, the blower command (activation/stop) depends on the temperature controller. The temperature controller is always computing the control signal $u_r[\cdot]$ that may become saturated at 0 or at $G_s[k]$. When the shutter is closed ($u_k[\cdot] = 0$) with $T_R[k] < T_s[k]$ ($e_s[k] < 0$) then the blower/fan is operating (ON) $u_{bf}[\cdot] = 100$. Considering the exact linearization controller, it starts to open the shutter before $e[\cdot] \geqslant 0$, the decision depends on $((1 + K_i h)e_s[k] - e_s[i-1]) > 0$). Depending on the evolution of $e_s[\cdot]$, for example if $e_s[\cdot]$ does not decrease, it is possible that at a future time p, the control $u_r[p] = 0$, and this will trigger the activation of the blower. This mechanism may raise questions about the closed-loop stability in

the presence of the switching. With active cooling, the actuator can be modelled as the concatenation of two linear functions, one for positive arguments, and the other for negative ones. If both these functions are inside a sufficient tight sector nonlinearity, by Lure's theorem (Khalil, 2002, p. 264), the controlled system will be asymptotically stable provided that the temperature controller assuming an ideal linear actuator is also asymptotically stable. This ensures that the oscillations will die out even in the presence of switching. This argument is confirmed by the results obtained.

5. Practical evaluation of active cooling with the exact linearization controller

The exact linearization controller is described in Appendix A.1, and the discrete time version is defined by the following equations,

$$\bar{u}_r[k] = \frac{\dot{T}_R[k] + \hat{\alpha}_1(T_R^4[k] - T_b^4) + \hat{\alpha}_2(T_R[k] - T_e)}{\hat{\alpha}_3}, \tag{16}$$

$$u_r[k] = \bar{u}_r[k] + \frac{K_I}{\hat{\alpha}_3}\left(e_s[k] + K_i \sum_{i=0}^{i=k} (e_s[i]h)\right), \tag{17}$$

where $\bar{u}_r[k]$ is a nonlinear feed-forward term, K_I and K_i are adjustable controller parameters (for the discrete time version of the controller) and $u_r[k]$ is the control signal to be applied to the shutter controller. Note that the integrator has an anti-windup mechanism (not included in the equations) to deal with the control signal saturation. A discrete time implementation of the continuous time controller is used.

Fig. 8 shows the results of an experiment (Exp.1) obtained with the exact linearization control law. The sample is made of stainless steel. The parameter estimates obtained from the sample to be tested $\bar{\alpha}_1$, $\bar{\alpha}_2$, and $\bar{\alpha}_3$ are respectively, 1.002×10^{-11}, 3.340×10^{-2}, 5.839×10^{-1}. These parameters are used in the feed-forward term of the control law. The controller gains were selected as $K_I = 0.4$, $K_i = 0.1$, and the sampling time is $h = 0.5$ s. The experimental results show that the controller is able to track the temperature reference, except during the decreasing phase of the reference where the control signal $u_s[\cdot]$, that commands the shutter, is saturated at 0%. During this period of time the heat loss caused by radiation and natural convection is not sufficient to decrease the temperature of the sample at the desired rate. Forced convection must therefore be used to increase the heat loss. The spikes that are present in the control during the decreasing of the temperature reference phase are caused by temperature reference changes. The feed-forward term of the control law employs the time derivative of the reference.

Fig. 9 shows the experimental results obtained with a stainless steel sample and using the same controller as in experiment 1, but in this case active cooling is applied automatically. The shutter command signal is represented in blue colour and is similar as in experiment 1. The blower command signal is represented in green colour and takes the values 0% or 100%. It can be concluded that by applying active cooling the temperature reference tracking is improved.

Figs. 10 and 11 show respectively the behaviour of the solar irradiance (solar power) and experimental results obtained with a "cofalit" material sample. In this experiment the controller parameter are $\bar{\alpha}_1 = 6.917 \times 10^{-12}$, $\bar{\alpha}_2 = 4.700 \times 10^{-3}$, $\bar{\alpha}_3 = 3.495 \times 10^{-1}$, $K_I = 0.5$, $K_i = 0.125$, and the sampling time is $h = 0.5$ s. It must be emphasized that active cooling was not used during the second temperature cycle and as a consequence it was not possible to track the reference at low temperature. It is also remarked that during the third cycle a huge drop on $G_s(t)$ unables reference tracking at high temperature, but the controller system is able to recover from that situation.

From the results obtained from this experiment it can be concluded that, although it provides a better performance, the cooling system must be improved to remove more heat. Additionally the sampling time must be decreased in order to obtain a rapid response during a rapid change in $G_s(\cdot)$.

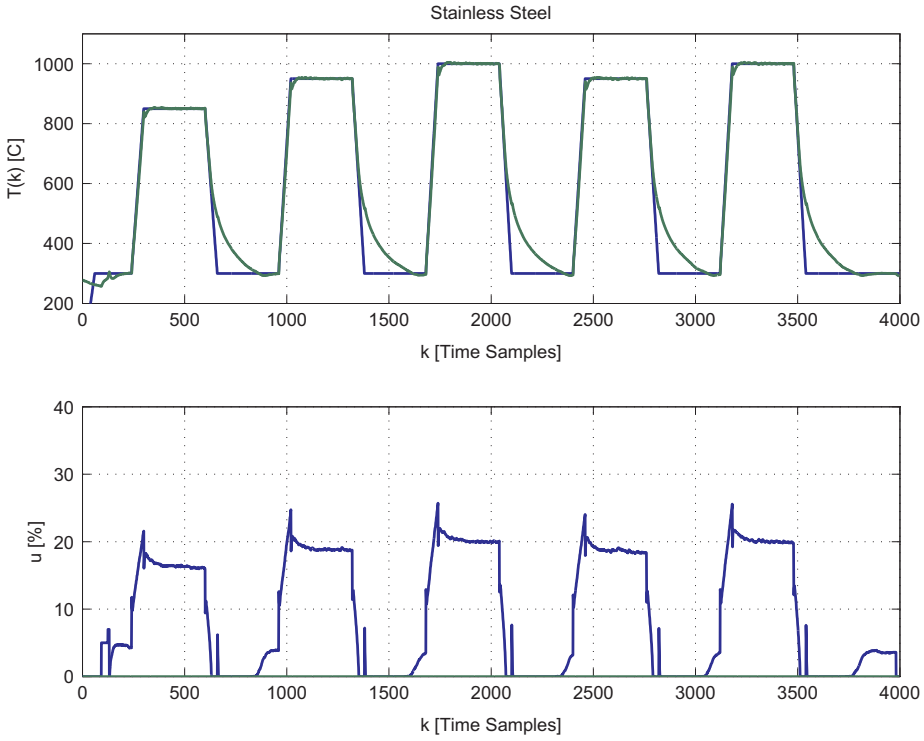

Fig. 8. Exp1: Temperature control of a stainless steel sample using the exact linearization controller, with $G_s[\cdot] \approx 980$ W/m^2.

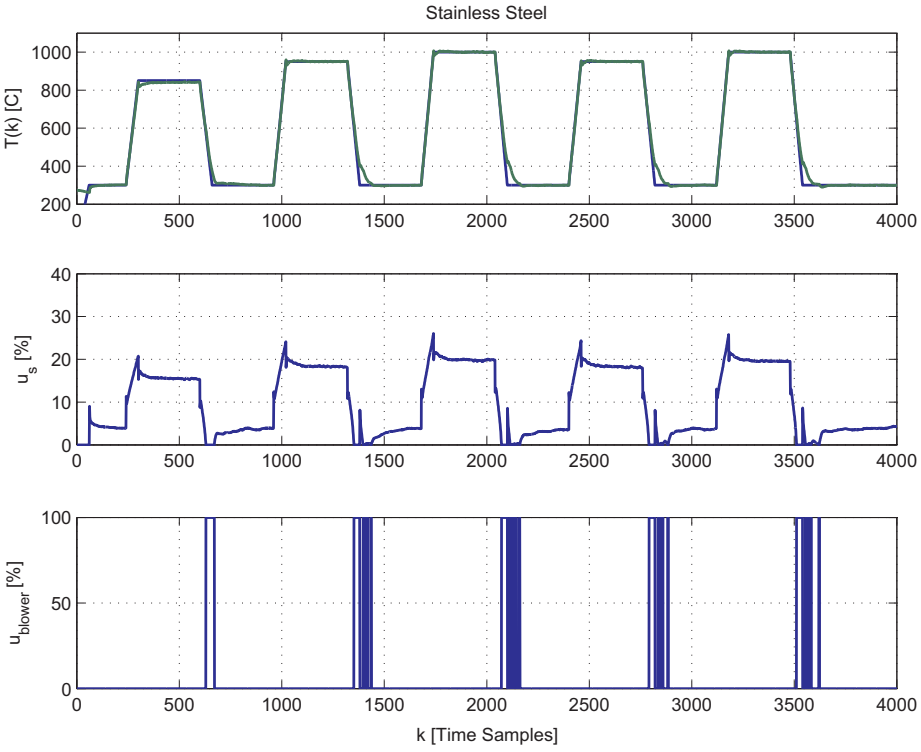

Fig. 9. Exp2: Temperature control of a stainless steel sample, as in Fig. 8, using the exact linearization controller and active cooling with $G_s[\cdot] \approx 1000$ W/m^2. The blower command operates in an on (0%)-off(100%) strategy.

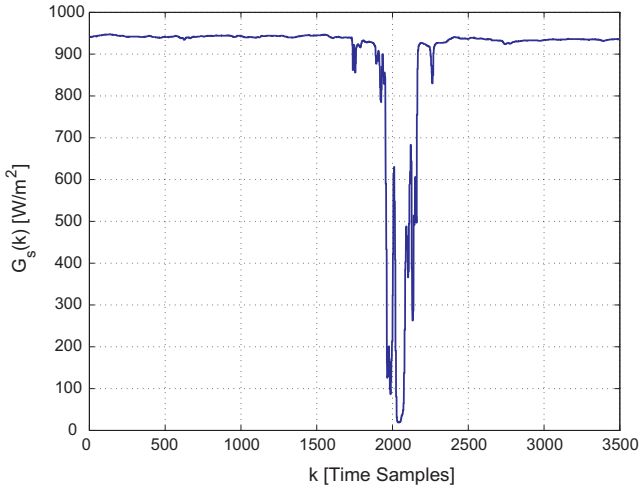

Fig. 10. Exp 3: Evolution of the sun power ($G_s[k]$) during an experiment with a "cofalit" material sample.

6. Practical evaluation of active cooling with MPC

In this section, experimental results obtained with a Model Predictive Controller (MPC) with Integral Action (described in Appendix A.2) and active cooling are shown. The MPC controller is described by the following discrete time equations,

$$\delta u_r[k] = K_1(T_s[k] - T_R[k]) + K_2(T_s[k] - T_s[k-1]), \quad (18)$$

$$u_r([k] = u_r[k-1] + \delta u_r[k], \quad (19)$$

where K_1 and K_2 are the controller parameters that are computed from the minimization of a cost function that is parameterized by the control horizon N and by the control weight ρ. The implementation of the discrete time integrator has an anti-windup mechanism. This mechanism is used when $u_r[k-1] + \delta u_r[k] < 0$ or $u_r[k-1] + \delta u_r[k] > u_{rmax}$ to adjusts the value of the integrator $u_r[k-1]$, such that $u_r(k) = 0$ or $u_r[k] = u_{rmax}$ respectively.

In experiment 4 the "cofalit" material is used. The controller parameters are computed from the process model, with the parameter estimates shown in experiment 3. Two sets of gains are tested, one for $\rho = 8$ ($K_1 = 0.2986, K_2 = -1.6138$) and the other for $\rho = 16$ ($K_1 = 0.2167, K_2 = -1.3773$). These gains are computed for a large time horizon ($N = 100$), and it is assumed that the temperature reference is $T_R = 1000$ [°C]. The results are presented in Fig. 12. During the first temperature cycle the first set of gains is used. They are changed to the second set of gains to obtain a smoother shutter control signal. Active cooling is not used in the first temperature cycle which shows that heat loss by radiation and by natural convection are not enough to allow temperature reference tracking. During the cycles 2, 3, and 4 the temperature tracking is improved with active cooling, but this action is still not able to remove the required amount of heat. In the last temperature cycle, the active cooling was delayed to show the rate of temperature decreasing with natural and with forced convection.

The last temperature cycle of the experiment is shown in Fig. 13 where the active cooling was delayed to put in evidence the natural and forced convection and the coordination between the two actuators.

In the last experiment, Exp.5, a 25 mm × 25 mm 10 mm SiC sample is tested using MPC and active cooling. During this experiment the solar power $G_s(t)$ is not constant (Fig. 14) and it is partially blocked by the presence of moving clouds. The temperature reference was selected according to the fact that SiC material is able to withstand very high temperatures but the temperature change must be "slow" since otherwise the sample breaks. The parameters of the heating process are

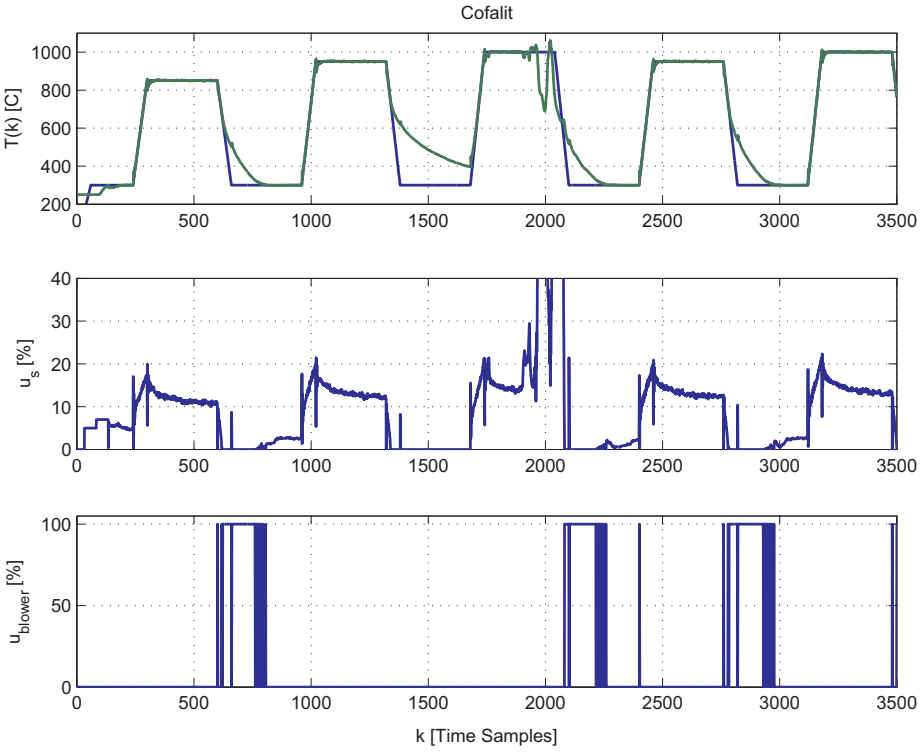

Fig. 11. Exp3: Temperature control of a "cofalit" sample, using the exact linearization controller with active cooling. Active cooling is not used during the second temperature cycle causing a degradation on the temperature tracking. A huge drop in $G_s[\cdot]$ occurs during the third cycle that unables the controller to track the reference.

$\overline{\alpha}_1 = 3.36 \times 10^{-12}$, $\overline{\alpha}_2 = 4.80 \times 10^{-3}$, $\overline{\alpha}_3 = 3.36 \times 10^{-1}$ and the controller parameters are $K_1 = 0.892$ and $K_2 = -9.335$. The results of this experiment are shown in Fig. 15. During the first temperature cycle, active cooling is not applied and the tracking is not possible for low temperatures. The non-smooth behaviour of the shutter control signal is caused by the controller that tries to compensate the changes of the sun power as it tracks the temperature reference.

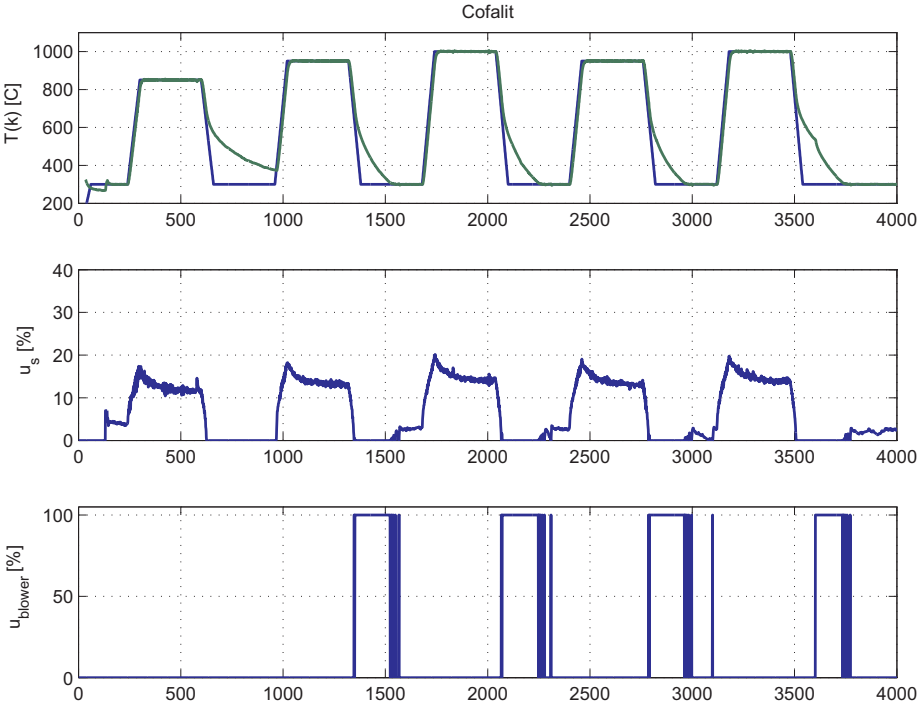

Fig. 12. Exp4: Temperature control of a "cofalit" sample using the MPC controller with active cooling. The temperature tracking is similar as the one shown in Fig. 11 but the shutter control signal is smoother. The solar power is 850 W/m^2 at the beginning of the experiment and increases linearly to 900 W/m^2 at the end of the experiment.

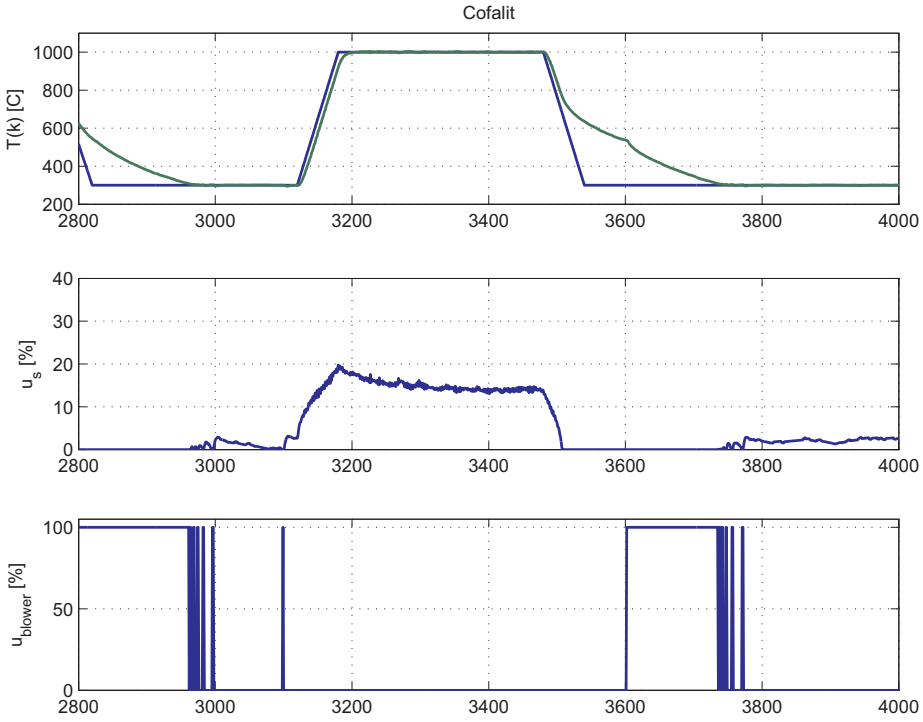

Fig. 13. Exp4: Temperature control of a "cofalit" sample using the MPC with active cooling, showing the last temperature cycle of the experiment 4. The active cooling was delayed to put in evidence the natural and forced convection and the coordination between the two actuators.

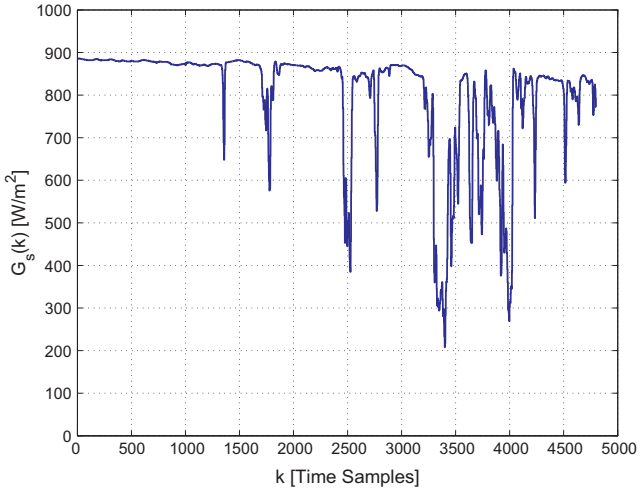

Fig. 14. Exp.5: Time behaviour of the sun power ($G_s(t)$) during an experiment with the SiC sample.

7. Conclusions

A control system architecture for small size solar furnaces is proposed and is evaluated in this article. The main control loop is dedicated to active heating, where the amount of power that is applied on the surface of the sample is adjusted by commanding the shutter. For situations when the temperature reference decreases too fast and the shutter is already closed, active cooling is employed to improve reference tracking. Two control methodologies are applied to design the temperature controller, one (exact linearization) uses a nonlinear feedforward term couple with a PI controller, while the other controller is designed using the model predictive control with integral action. Both controllers are evaluated in conjunction with active cooling that operates using a on-off strategy. Experimental results obtained with different material samples show that the proposed control system architecture is adequate to control solar furnaces with active cooling yielding a significant performance improvement when tracking time varying temperature references.

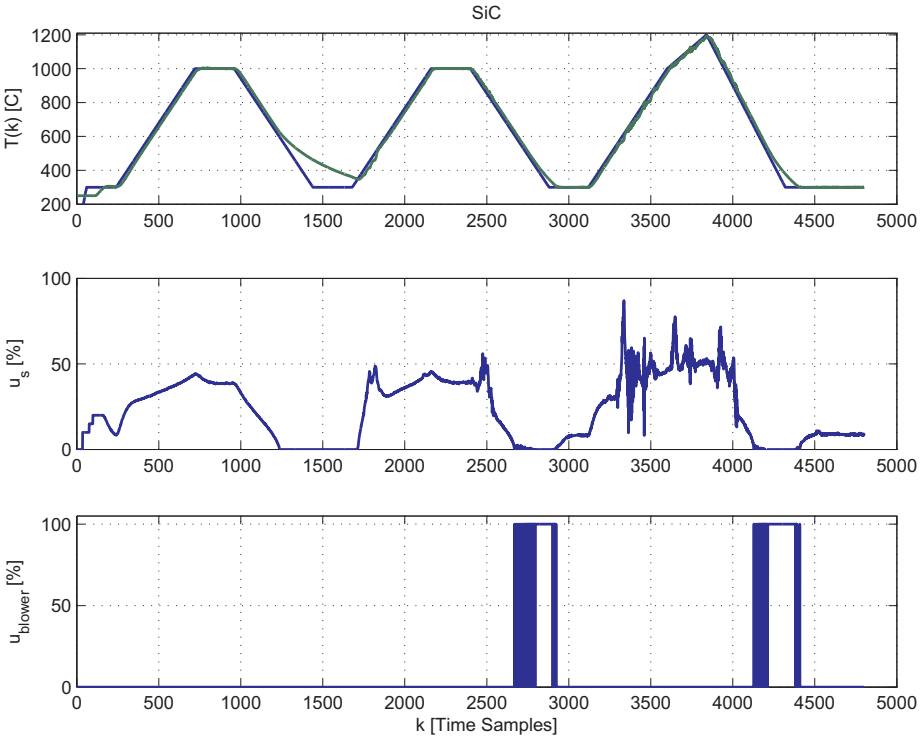

Fig. 15. Exp.5: Temperature control of a SiC sample using the MPC controller with active cooling. The non-smooth behaviour of the shutter control signal is caused by the controller that tries to compensate the changes in $G_s[k]$.

Appendix A. Temperature controller design

A.1. Control law based on the concept of exact linearization

The approach proposed (Costa et al., 2016b) is based on the definition of a virtual control input $u_r(t)$ such that $u_r(t) = G_s(t)s_{fs}(u_s(t))$. The aim is to impose $u_r(\cdot)$ and to invert the nonlinearity such that $u_s(\cdot)$ is computed and applied to the shutter. Note that $s_{fs}()$ is known and $G_s(t)$ is measured. Additionally, the proposed control will be based on the concept of exact linearization.

Define

$$e_s(t) \triangleq T_R(t) - T_s(t), \tag{A.1}$$

where $T_R(t)$ represents the temperature reference and define the tracking error dynamics $\dot{e}_s(t) \triangleq \dot{T}_R(t) - \dot{T}_s(t)$, that can be written as

$$\dot{e}_s(t) = \dot{T}_R(t) + \alpha_1[(T_R(t) - e_s(t))^4 - T_e^4(t)] + \alpha_2[T_R(t) - e_s(t) - T_e(t)] - \alpha_3 u_r(t). \tag{A.2}$$

Expanding the nonlinear term $(T_R(t) - e_s(t))^4$ as $T_R^4(t) - 4T_R^3(t)e_s(t) + 6T_R^2(t)e_s^2(t) - 4T_R(t)e_s^3(t) + e^4(t)$ and assuming that $e_s(t)$ is small enough such that $(T_R(t) - e_s(t))^4 \approx T_R^4(t) - 4T_R^3(t)e_s(t)$, then (A.2) can be approximated by

$$\dot{e}_s(t) = -[\alpha_1 4T_R^3(t) + \alpha_2]e_s(t) + \dot{T}_R(t) + \alpha_1[T_R^4(t) - T_e^4(t)] + \alpha_2[T_R(t) - T_e(t)] - \alpha_3 u_r(t). \tag{A.3}$$

Having the estimates $\hat{\alpha}_i$ of the process parameters α_i and estimates of the error bounds, such that $\alpha_i = \hat{\alpha}_i + \Delta\alpha_i$, the control signal is defined as $u_r(t) = \overline{u}_r(t) + \delta_r(t)$ with

$$\overline{u}_r(t) = \frac{\dot{T}_R(t) + \hat{\alpha}_1(T_R^4(t) - T_0^4) + \hat{\alpha}_2(T_R(t) - T_e)}{\hat{\alpha}_3} \tag{A.4}$$

where the term $\overline{u}_r(t)$ is used to cancel the nonlinear thermal dynamics. The dynamics of the tracking error can now be written as

$$\dot{e}_s(t) = \frac{\Delta\alpha_3}{\hat{\alpha}_3}\dot{T}_R(t) + \left(\Delta\alpha_1 + \hat{\alpha}_1\frac{\Delta\alpha_3}{\hat{\alpha}_3}\right)(T_s^4(t) - T_e^4(t)) + \left(\Delta\alpha_2 + \hat{\alpha}_2\frac{\Delta\alpha_3}{\hat{\alpha}_3}\right)(T_s(t) - T_e(t)) - \alpha_3\delta_r(t). \tag{A.5}$$

The input $\delta_r(t)$ is used to compensate small parameter errors. Defining $\delta_r(t) = K_l/\hat{\alpha}_3(e_s(t) + K_i\int(e_s(\tau)d\tau)$ and considering that the $\Delta\alpha_i$ are small, the dynamics of the tracking error can be written as

$$\dot{e}_s(t) = -\frac{\alpha_3}{\hat{\alpha}_3}K_l(e_s(t) + K_i\int_0^t(e_s(\tau)d\tau). \tag{A.6}$$

The parameters of the PI controller can now be selected such the dynamics of the tracking error (A.6) is stable without overshooting and a null static error. It is remarked that the terms of (A.5) that depend on $\Delta\alpha_i$ can be evaluated for the temperature reference profile and bounds can be computed and used to evaluate the robustness of the controller. A possible algorithm to select the PI controller parameters is to imposed a real double pole on the tracking error dynamics, where $K_i = 0.25{*}K_l$. A discrete time version of the controller equations is implemented with a small sampling time compared with the time constant of the process. That provides a good approximation of the continuous time controller.

A.2. Control law based on minimization of a cost function

The control law (Costa et al., 2016a) is design based on the minimization of the cost function

$$J(N) = \sum_{j=1}^{N} [(T_s(k+j) - T_R(k+j))^2 + \rho(\delta u_r(t+j-1))^2], \tag{A.7}$$

where N defines the control horizon corresponding to the time window Nh, with h being the sampling interval and k represents discrete time. $T_R(\cdot)$ represents the future temperature profile, $T_s(\cdot)$ represents the output of the process to be controlled, and $\rho > 0$ is an adjustable parameter that weights the future incremental control actions $\delta u_r(\cdot)$, (Camacho, 2007; Kwon and Han, 2005).

In order to compute the predictors that relate the process output $T_s(\cdot)$ with the control increment $\delta u_r(\cdot)$ one considers the discrete time version of (4)

$$T_s(k+1) = T_s(k) - h\overline{\alpha}_1[T_s^4(k) - T_b^4] - h\overline{\alpha}_2[T_s(k) - T_e] + h\overline{\alpha}_3 u_r(k), \tag{A.8}$$

where $u_r(k) = G_s(k)s_{fs}(u_s(k))$. Considering (A.8) at time k and defining now the operation $\delta T_s(k+1) = T_s(k+1) - T_s(k)$, an incremental model of the process is obtained that eliminates constant terms such as T_b and T_e,

$$\delta T_s(k+1) = \delta T_s(k) - h\overline{\alpha}_1[T_s^4(k) - T_s^4(k-1)] - h\overline{\alpha}_2\delta T_s(k) + h\overline{\alpha}_3\delta u_r(k), \tag{A.9}$$

where the nonlinear term $T_s^4(k) - T_s^4(k-1)$ can be approximated by a Taylor expansion

$$T_s^4(k) - T_s^4(k-1) \simeq 4T_s^3(k-1)\delta T_s(k).$$

Assuming that the tracking error is small, the term $T_s^3(k-1)$ can be replaced by the reference $T_R^3(k-1)$ and, the incremental model given by Eq. (A.9) is written as

$$\delta T_s(k+1) = \Phi(k+1,k)\delta T_s(k) + \Gamma\delta u_r(k), \tag{A.10}$$

$$T_s(k+1) = T_s(k) + \delta T_s(k+1), \tag{A.11}$$

where

$$\Phi(k+1,k) = 1 - h\overline{\alpha}_1 4T_R^3(k-1) - h\overline{\alpha}_2, \tag{A.12}$$

$$\Gamma = h\overline{\alpha}_3. \tag{A.13}$$

The output predictors from $k+1$ to $k+N$ can now be computed using (A.10) and (A.11).

$$\begin{aligned}
\delta T_s(k+1) &= \Phi(k+1,k)\delta T_s(k) + \Gamma\delta u_r(k)\\
\delta T_s(k+2) &= \Phi(k+2,k+1)\delta T_s(k+1) + \Gamma\delta u_r(k+1)\\
\delta T_s(k+3) &= \Phi(k+3,k+2)\delta T_s(k+2) + \Gamma\delta u_r(k+2)\\
&\dots = \dots\\
\delta T_s(k+N) &= \Phi(k+N,k+N-1)\delta T_s(k+N-1) + \Gamma\delta u_r(k+N-1)
\end{aligned}$$

$$\begin{aligned}
T_s(k+1) &= T_s(k) + \delta T_s(k+1)\\
T_s(k+2) &= T_s(k) + \delta T_s(k+1) + \delta T_s(k+2)\\
T_s(k+3) &= T_s(k) + \delta T_s(k+1) + \delta T_s(k+2) + \delta T_s(k+3)\\
&\dots = \dots\\
T_s(k+N) &= T_s(k) + \delta T_s(k+1) + \dots + \delta T_s(k+N)
\end{aligned}$$

$$T_s(k+1) = T_s(k) + \Phi(k+1,k)\delta T_s(k) + \Gamma\delta u_r(k) \tag{A.14}$$

$$\begin{aligned}
T_s(k+2) = T_s(k) &+ \Phi(k+1,k)\delta T_s(k) + \Gamma\delta u_r(k)\\
&+ \Phi(k+2,k+1)\Phi(k+1,k)\delta T_s(k)\\
&+ \Phi(k+2,k+1)\Gamma\delta u(k) + \Gamma\delta u_r(k+1)
\end{aligned} \tag{A.15}$$

$$T_s(k+3) = \dots \tag{A.16}$$

Rearranging the terms, the predictors can be written in a matrix equation that has the following form,

$$T_p = I_{n,1}T_s(k) + S\delta T_s(k) + W\delta U_r, \tag{A.17}$$

where

$$T_p = [T_s(k+1)\ T_s(k+2) \dots T_s(k+N)]',$$

$$I_{(n,1)} = [1\ 1\ \dots\ 1]'$$

S is a column vector and W is a square matrix, and

$$\delta U_r = [\delta u_r(k)\ \delta u_r(k+1)\ \dots\ \delta u_r(k+N-1)].$$

Using (A.17) in the cost function (A.7), and minimizing it with respect to the incremental control actions, the future incremental control actions are given by

$$\delta U_r = -(W'W + \rho I)^{-1}W'[I_{n,1}T_s(k) - T_R + S\delta T_s(k)]. \tag{A.18}$$

According to a receding horizon strategy only the first value of δU_r, that is $\delta u_r(k)$, is applied to the process (Camacho, 2007; Kwon and Han, 2005).

The equations that define the control law are

$$\delta u_r(k) = K_1(T_s(k) - T_R(k)) + K_2(T_s(k) - T_s(k-1)), \tag{A.19}$$

$$u_r(k) = u_r(k-1) + \delta u_r(k), \tag{A.20}$$

and

$$u_s(k) = s_{fs}^{-1}(u_r(k)/G_s(k)), \tag{A.21}$$

that is used to compensate the static function of the shutter and the sun power variability. Note that, in order to simplify the controller implementation, the controller gains are computed off-line and an anti-windup mechanism is used to readjust the control when it is saturated.

The robustness of the control algorithm can be analysed using the methodology described in Stoica et al. (2007).

References

Agrafiotis, C., von Storch, H., Roeb, M., Sattler, C., 2014. Solar thermal reforming of methane feedstocks for hydrogen and syngas production: a review. Renew. Sustain. Energy Rev. 29 (0), 656–682.

Berenguel, M., Camacho, E., Garcia-Martin, F., Rubio, F., 1999. Temperature control of a solar furnace. IEEE Control Syst. 19 (1), 8–24.

Beschi, M., Visioli, A., Berenguel, M., Yebra, L., 2012. Constrained temperature control of a solar furnace. IEEE Trans. Control Syst. Technol. 20, 1263–1274.

Beschi, M., Berenguel, M., Visioli, A., Guzman, J.L., Yebra, L., 2013a. Implementation of feedback linearization GPC control for a solar furnace. J. Process Control 23, 1545–1554.

Beschi, M., Berenguel, M., Visioli, A., Yebra, L., 2013b. Constrained control strategies for disturbance rejection in a solar furnace. Control Eng. Pract. 21, 1410–1421.

Beschi, M., Padula, F., Visioli, A., 2016. Fractional robust PID control of a solar furnace. Control Eng. Pract. 56, 190–199.

Camacho, E.F., 2007. Model Predictive Control, second ed. Springer.

Camacho, E., Rubio, F., Berenguel, M., Valenzuela, L., 2007a. A survey on control schemes for distributed solar collector fields. Part I: modeling and basic control approaches. Sol. Energy 81 (10), 1240–1251.

Camacho, E., Rubio, F., Berenguel, M., Valenzuela, L., 2007b. A survey on control schemes for distributed solar collector fields. Part II: advanced control approaches. Sol. Energy 81 (10), 1252–1272.

Çengel, Y.A., 2003. Heat Transfer – A Practical Approach, second ed. McGraw-Hill, New York.

Costa, B.A., Lemos, J.M., 2009a. An adaptive temperature control law for a solar furnace. Control Eng. Pract. 17, 1157–1173.

Costa, B.A., Lemos, J.M., 2009b. Singular perturbation stability conditions for adaptive control of a solar furnace with actuator dynamics. In: Proc. European Control Conference 2009 Budapest Hungary. pp. 1626–1631.

Costa, B.A., Lemos, J.M., 2012. Predictive adaptive temperature control in a solar furnace for material stress tests. In: Proc. IEEE Multi-conference on Systems and Control 2012 Dubrovnik Croatia. pp. 1340–1345.

Costa, B.A., Lemos, J.M., 2016. Optimal control of the temperature in a solar furnace. Opt. Control Appl. Methods 37, 466–478.

Costa, B.A., Lemos, J.M., Rosa, L.G., 2011. Temperature control of a solar furnace for material testing. Int. J. Syst. Sci. 42, 203–206.

Costa, B.A., Lemos, J.M., Guillot, E., 2016a. Control of a solar furnace using MPC with integral action. In: Proc. 11th IFAC Symposium on Dynamics and Control of Process Systems 2016 Trondheim Norway. pp. 961–966.

Costa, B.A., Lemos, J.M., Guillot, E., 2016b. Control of a solar furnace using active cooling. In: Proc. European Control Conference 2016 Aalborg Denmark. pp. 19–24.

Khalil, H.K., 2002. Nonlinear Systems, third ed. Prentice-Hall.

Kwon, W.H., Han, S., 2005. Receding Horizon Control-Model – Predictive Control for State Models. Springer.

Oliveira, F.A.C., Rosa, L.G., Fernandes, J.C., et al., 2015. Nitriding VI-group metals (Cr, Mo and W) in stream of NH_3 gas under concentrated solar irradiation in a solar furnace at PSA. Sol. Energy 114, 51–60.

Oliveira, F., Fernandes, J., Rodriguez, J., Canadas, I., Galindo, J., Rosa, L., 2016. Temperature uniformity improvement in a solar furnace by indirect heating. Sol. Energy 140, 141–150.

Stephanopoulos, G., 1984. Chemical Process Control – An Introduction to Theory and Practice. Prentice-Hall International Edition.

Stoica, C., Rodriguez-Ayerbe, P., Dumur, D., 2007. Off-line robustness improvement of predictive control laws in state-space description. In: Proc. Control Automation, 2007. MED '07. Mediterranean Conference on. pp. 1–6.